Modular Dynamic Model for Multi-Three-Phase Electrically Excited Synchronous Machines

Modular Dynamic Model for Multi-Three-Phase Electrically Excited Synchronous Machines

Lorenzo Perilli, *Student Member*, *IEEE*
Dipartimento Energia
Politecnico di Torino
Turin, Italy
lorenzo.perilli@polito.it

Federica Graffeo, *Member*, *IEEE*
Dipartimento Energia
Politecnico di Torino
Turin, Italy
federica.graffeo@polito.it

Sandro Rubino, *Member*, *IEEE*
Dipartimento Energia
Politecnico di Torino
Turin, Italy
sandro.rubino@polito.it

Alberto Tenconi
Dipartimento Energia
Politecnico di Torino
Turin, Italy
alberto.tenconi@polito.it

Silvio Vaschetto, *Senior Member*, *IEEE*
Dipartimento Energia
Politecnico di Torino
Turin, Italy
silvio.vaschetto@polito.it

***Abstract*—Multi-three-phase electrically excited synchronous machines can enable the electrification of applications featuring stringent requirements in terms of fault tolerance and reliability, as in the aerospace industry and in sustainable energy generation. Indeed, the presence of multiple stator three-phase winding sets improves both redundancy and operational safety. Moreover, the regulation of the excitation achieved by means of the rotor winding enables the possibility of completely de-energizing the machine in case of faults. Furthermore, the rotor current regulation allows achieving high efficiency and power factor in a wide speed range. However, multiple stator three-phase sets and the presence of a variable rotor current result in nontrivial dynamic modeling, particularly when considering the iron saturation nonlinearities. In this framework, a multi-stator formulation for the nonlinear dynamic modeling of the multi-three-phase electrically excited synchronous machine is developed. The multi-stator approach interacts with a separate rotor model for the computation of the excitation flux linkage dynamics. The accuracy and capabilities of the proposed model in representing fault conditions are evaluated in simulation using the data of a quadruple-three-phase motor.**

Keywords—electrically excited synchronous motor, multi-three-phase machines, dynamic modeling, multi-stator model, flux maps.

I. Introduction

The path toward the electrification of the transport industry, especially the aircraft sector, and sustainable energy conversion, such as the offshore wind generation, requires advancements in fault-tolerant and reliable electric machines and drives [1]-[6]. The stringent fault tolerance and safety requirements demanded by these applications can be achieved by means of multi-three-phase machine configurations, in which the stator has multiple three-phase winding sets [7]-[9]. In this regard, the individual contributions of each set to the total flux and torque productions increase the redundancy of the electric machine [10]-[12].

Among the main multi-three-phase machine characteristics, there is the possibility of reducing the per-phase current rating for a given power, compared to three-phase machines [13], [14]. Indeed, multiple winding sets allow reducing the phase current, without increasing the corresponding phase voltage, particularly in high-power applications. Moreover, conventional three-phase

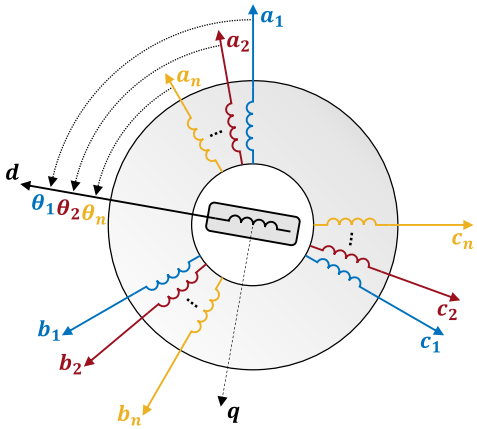

Fig. 1. Schematic representation of a 2-pole multi-three-phase EESM.

DC/AC power electronics converters can also be used for the stator supply [15], [16]. Furthermore, the modularity associated with multi-three-phase machine stators enables straightforward reconfiguration of the drives in the event of an open-phase fault, in which the faulty three-phase unit can be disconnected from the power supply [17], [18]. Finally, reduced torque pulsations can be obtained with multi-three-phase machine configurations in healthy conditions and the low torque ripple can be preserved in the post-fault operation for weak magnetic couplings between the stator sets [19], [20].

For particularly safety-critical applications, the electrically excited synchronous machine (EESM) topology benefits from intrinsic fail-safe characteristics [21], [22]. Indeed, the machine peculiarity consists of the controllability of the excitation field, provided by the rotor winding [23]. In the case of a stator fault, the possibility of promptly acting on the field current enhances both the reliability and the safety of the multi-three-phase drive [24]. Moreover, the excitation flux can be regulated to improve the performance at partial load, as well as to widen the constant power speed range [25]. In order to overcome the challenges of the excitation current supply, many research activities have been focusing on developing low-maintenance, brushless systems for the rotor circuit [21]-[23].

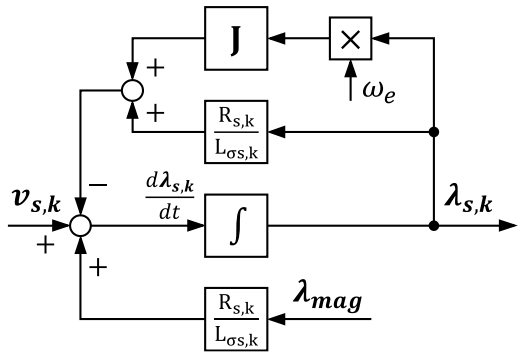

Fig. 2. Electromagnetic *dq* model of the stator *k*-th three-phase winding.

The implementation of accurate dynamic models for multi-three-phase EESMs constitutes an essential tool for numerical simulations [26]. However, the contribution of the literature to the dynamic modeling of multi-three-phase electrically excited synchronous machines considering the nonlinearities is limited. These dynamic models are needed to develop control algorithms and to analyze the drive performance in the case of faults, when one or more stator three-phase sets are excluded from the total flux and torque productions [27]. For this purpose, the modeling approach must be capable of simulating the different machine fault conditions, while also representing the magnetic saturation occurring in the iron core. The scenario is further complicated by the presence of the rotor current, constituting an additional control variable for the multi-three-phase EESMs, with respect to the other machine types.

In this paper, a dynamic modeling approach for multi-three-phase electrically excited synchronous machines is proposed. The modularity of the developed model, consisting of separate blocks for the different machine windings, is achieved by means of the multi-stator (MS) formulation, which permits highlighting flux and torque contributions of each stator three-phase set [17]. In addition, the MS approach constitutes a convenient method to simulate the disconnection of the three-phase sets following an open-phase fault. High fidelity in representing the nonlinearities of the iron saturation is obtained using flux-error maps, which are derived from the current-to-flux maps, i.e., the relationships between the stator and rotor flux linkages and currents. The MS model interacts with a separate rotor electromagnetic model to simulate the rotor dynamics, considering also the nonlinearities and enhancing the modularity of the EESM modeling approach. Finally, the results accuracy and the machine model capabilities in simulating the fault conditions are analyzed in a state-variable based environment, namely MATLAB/Simulink, using the data of a quadruple-three-phase EESM prototype obtained by finite element simulations.

II. Multi-Stator Formulation

The multi-stator dynamic model of the EESM is derived by applying the Clarke and Park transformations to the equations in phase variables of each stator three-phase winding unit. In this way, the electromagnetic variables of the sets are all referred to the *dq* reference frame, in which the *d*-axis corresponds to the rotor winding magnetic axis. For every unit, a different angle θ_k is used for the Park transformation, as highlighted in Fig. 1 for a representative 2-pole machine. In addition, the proposed model can be adopted for the simulations of multi-three-phase EESMs with symmetrical or asymmetrical stator windings [28].

Neglecting the iron losses, in an EESM with a number n of three-phase stator winding sets, the dynamic equation of the MS formulation in the rotating *dq* reference frame, for the *k*-th set ($k = 1, 2, \dots, n$), consists of:

$$\boldsymbol{v_{s,k}} = \mathrm{R_{s,k}}\, \boldsymbol{i_{s,k}} + \frac{d\boldsymbol{\lambda_{s,k}}}{dt} + \omega_e\, \mathbf{J}\, \boldsymbol{\lambda_{s,k}} \tag{1}$$

where $\boldsymbol{v_{s,k}}$, $\boldsymbol{i_{s,k}}$ and $\boldsymbol{\lambda_{s,k}}$ are vectors containing the *d*- and *q*-voltages, currents and flux linkages, respectively, in the form $\boldsymbol{x_{s,k}} = [x_{d,k};\, x_{q,k}]$. $\mathrm{R_{s,k}}$ is the *k*-th winding resistance, ω_e is the electrical pulsation and $\mathbf{J} = [0, -1;\, 1,\, 0]$. In order to solve (1), the current $\boldsymbol{i_{s,k}}$ is retrieved by means of (2), in which $\mathrm{L_{\sigma s,k}}$ is the leakage inductance of the *k*-th set and $\boldsymbol{\lambda_{mag}}$ is the magnetizing flux linkage of the stator, generated by the combined action of all the three-phase units and of the rotor winding.

$$\boldsymbol{\lambda_{s,k}} = \mathrm{L_{\sigma s,k}}\, \boldsymbol{i_{s,k}} + \boldsymbol{\lambda_{mag}} \tag{2}$$

The current vector expression can be also directly substituted into (1), leading to the stator *k*-th set model in (3) represented by the scheme in Fig. 2. As it can be observed, $\boldsymbol{\lambda_{mag}}$ is needed in the computation of the flux linkage time derivative for the stator *k*-th three-phase unit.

$$\frac{d\boldsymbol{\lambda_{s,k}}}{dt} = \boldsymbol{v_{s,k}} + \frac{\mathrm{R_{s,k}}}{\mathrm{L_{\sigma s,k}}}\, \boldsymbol{\lambda_{mag}} - \frac{\mathrm{R_{s,k}}}{\mathrm{L_{\sigma s,k}}}\, \boldsymbol{\lambda_{s,k}} - \omega_e\, \mathbf{J}\, \boldsymbol{\lambda_{s,k}} \tag{3}$$

For the purpose of the model implementation including iron saturation, the current-to-flux maps constitute the starting point of the procedure. For each stator three-phase winding, the maps can be expressed as:

$$\begin{cases} \lambda_{d,k} = \lambda_{d,k}\left(\sum_k i_{d,k}\,, \sum_k i_{q,k}\,, i_f\right) \\ \lambda_{q,k} = \lambda_{q,k}\left(\sum_k i_{d,k}\,, \sum_k i_{q,k}\,, i_f\right) \end{cases} \tag{4}$$

in which the flux linkage, with both leakage and magnetizing contributions, is a function of all the stator *d*- and *q*- currents and of the rotor field *f*- current. In this regard, the magnetizing flux linkage can be retrieved for the different operating conditions:

$$\begin{cases} \lambda_{mag,d} = \lambda_{d,k}\left(\sum_k i_{d,k}\,, \sum_k i_{q,k}\,, i_f\right) - \mathrm{L_{\sigma s,k}}\, i_{d,k} \\ \lambda_{mag,q} = \lambda_{q,k}\left(\sum_k i_{d,k}\,, \sum_k i_{q,k}\,, i_f\right) - \mathrm{L_{\sigma s,k}}\, i_{q,k} \end{cases} \tag{5}$$

During the simulation, the $\boldsymbol{\lambda_{mag}}$ needed to compute the state variable time derivative in (3) is expressed as:

$$\boldsymbol{\lambda_{mag}} = \boldsymbol{\lambda_{sf}} + \mathbf{M_{dq}} \sum_k \boldsymbol{i_{s,k}} - \boldsymbol{\Delta\lambda_{mag}} \tag{6}$$

in which the maps corresponding to the right-hand side terms are determined prior to the simulation, using the stator maps in (5). In particular, $\boldsymbol{\lambda_{sf}}$ in (6) is the part of stator magnetizing flux linkage generated by the field winding, equal to:

$$\boldsymbol{\lambda_{sf}} = \left[\lambda_{mag,d}(0,0,i_f);\, 0\right] \tag{7}$$

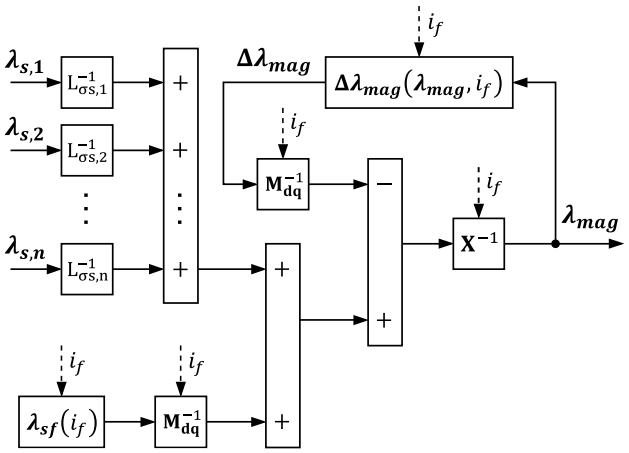

Fig. 3. Computation of the stator magnetizing flux linkage.

Moreover, $\mathbf{M_{dq}}$ is a 2×2 diagonal matrix storing the *d*- and *q*- stator magnetizing inductances:

$$\begin{cases} \mathrm{M_d} = \dfrac{\lambda_{mag,d}\left(\sum_k i_{d,k}, 0, i_f\right) - \lambda_{sf,d}}{\sum_k i_{d,k}} \\ \mathrm{M_q} = \dfrac{\lambda_{mag,q}\left(0, \sum_k i_{q,k}, i_f\right)}{\sum_k i_{q,k}} \end{cases} \tag{8}$$

The calculation of $\mathrm{M_d}$ and $\mathrm{M_q}$ for the different field currents can be performed for any *d*- or *q*- stator current values. However, the unsaturated condition represents the most convenient choice for (8), as it minimizes the interpolation errors at the borders of the model maps during the simulations. Indeed, the choice of the $\mathbf{M_{dq}}$ strongly affects the $\boldsymbol{\Delta\lambda_{mag}}$ values. The sum of (7) with the product of currents and magnetizing inductances will hereinafter be referred to as *'reference model'*, characterized by an intrinsic deviation with respect to the current-to-flux relationships in (5), depending on the machine operating point.

Finally, $\boldsymbol{\Delta\lambda_{mag}}$ consists of the *d*- and *q*-axis flux-error maps and compensates for the deviation between reference model and the magnetizing flux linkage in (6) [29]. The flux-error maps are derived in the form of 3-D maps, as functions of the magnetizing flux linkage components and of the rotor current. However, the maps need manipulation to be included in the simulation model, so as to take into account the effects of the variable rotor current on the interpolation domain. The detailed elaboration procedure to determine the flux-error maps is provided in Section III.

In this framework, the stator current vector derived using (2) can be substituted into (6), thus leading to the formulation in (9) for the magnetizing flux linkage.

$$\boldsymbol{\lambda_{mag}} = \mathbf{X}^{-1}\left(\mathbf{M_{dq}^{-1}}\,\boldsymbol{\lambda_{sf}} + \sum_k \frac{\boldsymbol{\lambda_{s,k}}}{\mathrm{L_{\sigma s,k}}} - \mathbf{M_{dq}^{-1}}\,\boldsymbol{\Delta\lambda_{mag}}\right) \tag{9}$$

In (9), $\mathbf{X} = \mathbf{M_{dq}^{-1}} + \sum_k\left(\mathrm{L_{\sigma s,k}^{-1}}\,\mathbb{1}_{2\times2}\right)$ for clarity reasons, being $\mathbb{1}_{2\times2}$ the identity matrix. Moreover, it is important to notice that, during the model numerical integration, the *d*- and *q*- flux-errors correspond to the previous simulation time instant. Indeed, the magnetizing flux linkage is needed to retrieve $\boldsymbol{\Delta\lambda_{mag}}$, as shown by the scheme in Fig. 3.

Regarding the advantages of the multi-stator dynamic model and the introduction of the magnetizing flux linkage term, there is the opportunity to separate the contribution $T_{e,k}$ of each three-phase unit to the total machine electromagnetic torque. Indeed, starting from the conventional torque calculation with the cross-product between the flux linkage and current vectors, the current determined using (2) can be substituted into the cross-product, leading to (10) for the contribution of the *k*-th three-phase set, in which p is the number of pole pairs of the machine.

$$T_{e,k} = \frac{3}{2}p\left(\boldsymbol{\lambda_{s,k}} \wedge \boldsymbol{i_{s,k}}\right) = \frac{3}{2}p\left(\frac{\boldsymbol{\lambda_{mag}} \wedge \boldsymbol{\lambda_{s,k}}}{\mathrm{L_{\sigma s,k}}}\right) \tag{10}$$

As it can be noted, the current vectors of the three-phase sets are not needed to solve the stator model, since the $\boldsymbol{i_{s,k}}$ are always replaced using (2). However, as detailed in Section IV, the stator currents are needed to interpolate the multidimensional maps of the rotor model, so as to compute the electromagnetic dynamics of the field winding variables.

In addition, the proposed MS formulation is characterized by enhanced simulation capabilities for the representation of faults. Indeed, the stator unit disconnection following the occurrence of a fault can be simulated performing the summations in (9) only for the active sets n_{active}. In this way, the units in open-circuit are excluded from the machine flux and torque productions.

Furthermore, the developed modular approach for the stator modeling including iron saturation is suitable for the numerical simulation of multi-three-phase EESM with different resistances and leakage inductances among the three-phase sets. This allows taking into account the differences in the parameters which can be measured by means of experimental tests.

III. Stator Flux-error Maps

In order to improve the numerical efficiency of the proposed flux-error approach, the $\boldsymbol{\Delta\lambda_{mag}}$ maps must be determined for a domain containing regularly spaced *d*- and *q*- stator magnetizing flux linkages, as expressed by (11).

$$\boldsymbol{\Delta\lambda_{mag}} = \boldsymbol{\Delta\lambda_{mag}}(\boldsymbol{\lambda_{mag}}, i_f) \tag{11}$$

Starting from (6), the flux-error maps can be computed for a regular grid of stator *d*- and *q*- currents. The main reason for the introduction of the magnetizing flux linkages consists of using the *d*- and *q*- components of $\boldsymbol{\lambda_{mag}}$ in the $\boldsymbol{\Delta\lambda_{mag}}$ determination, instead of all the currents in the stator three-phase sets from the previous simulation time instant.

Moreover, to improve the model accuracy and to reduce the computational burden, the flux-error maps formulation must be capable of considering the effect of the variable rotor current on the boundaries of the interpolation domain. For this purpose, a method similar to those developed in [26] and [30] is applied, in which the domain of the multidimensional maps is regularized and normalized for each value of the rotor current.

Regarding the domain of the *d*- and *q*- flux-error maps, two rounds of interpolation are performed, also iterating over all the values of rotor current. The regular grid of *d*- and *q*- currents for which $\boldsymbol{\Delta\lambda_{mag}}$ can be determined corresponds to a $\boldsymbol{\lambda_{mag}}$ domain

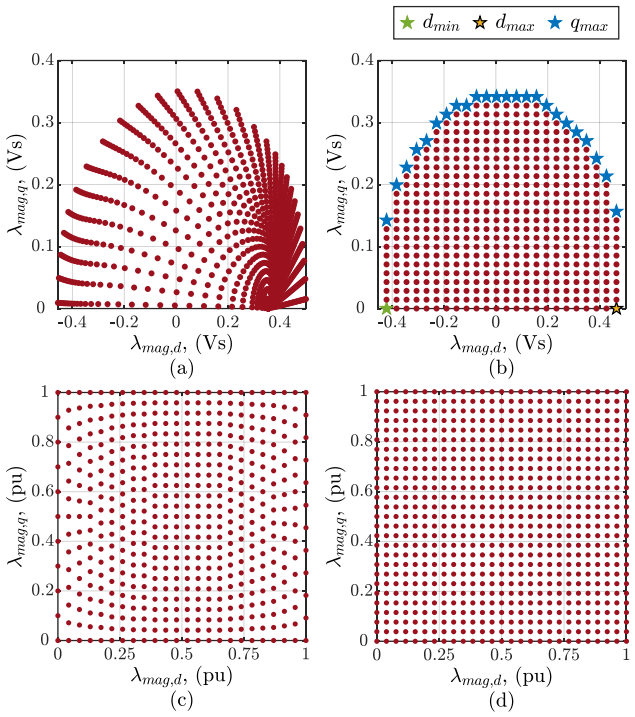

Fig. 4. Flux-error maps domain: (a) magnetizing fluxes for a regular current grid at positive rotor current, (b) regularized domain, (c) normalized domain, (d) regularized and normalized domain.

with non-regularly spaced elements, due to the iron saturation. Therefore, a regular grid of d- and q- magnetizing flux linkages is defined and the corresponding $\boldsymbol{\Delta\lambda_{mag}}$ values are obtained by means of the first interpolation. The domain points for a regular current grid and the results of the first interpolation are presented in Fig. 4a and Fig. 4b, respectively, for a positive rotor current.

The second interpolation is performed to consider the effect of the rotor current on the boundaries of the regular magnetizing flux grid. Indeed, for different excitations, the $\boldsymbol{\lambda_{mag}}$ boundaries in Fig. 4b change, as the i_f varies. Therefore, the minimum and maximum d- and q- components of the magnetizing flux linkage are determined. It is important to notice that the minimum and maximum $\lambda_{mag,d}$ depend solely on the rotor current, while the maximum $\lambda_{mag,q}$ depends also on the $\lambda_{mag,d}$ value.

Finally, the domain of magnetizing flux linkage components is normalized. However, the normalization procedure does not preserve the regularly spaced grid, as shown in Fig. 4c. Thus, a second interpolation of the $\boldsymbol{\Delta\lambda_{mag}}$ values is needed to obtain a regular domain for (11), in which the $\boldsymbol{\lambda_{mag}}$ elements are equally spaced and do not change with the rotor current. The regularized and normalized grid is presented in Fig. 4d. The boundaries of the domain are also used in the simulation for the normalization of $\boldsymbol{\lambda_{mag}}$, to retrieve the flux-errors by means of (11).

The $\boldsymbol{\Delta\lambda_{mag}}$ for a positive rotor current is shown in Fig. 5. In order to provide a straightforward explanation of the behavior for the flux-error maps, the domain of Fig. 4b has been chosen. As it can be observed in Fig. 5a, the d-axis component of $\boldsymbol{\Delta\lambda_{mag}}$ is close to zero for low $\lambda_{mag,d}$ values, since the reference model

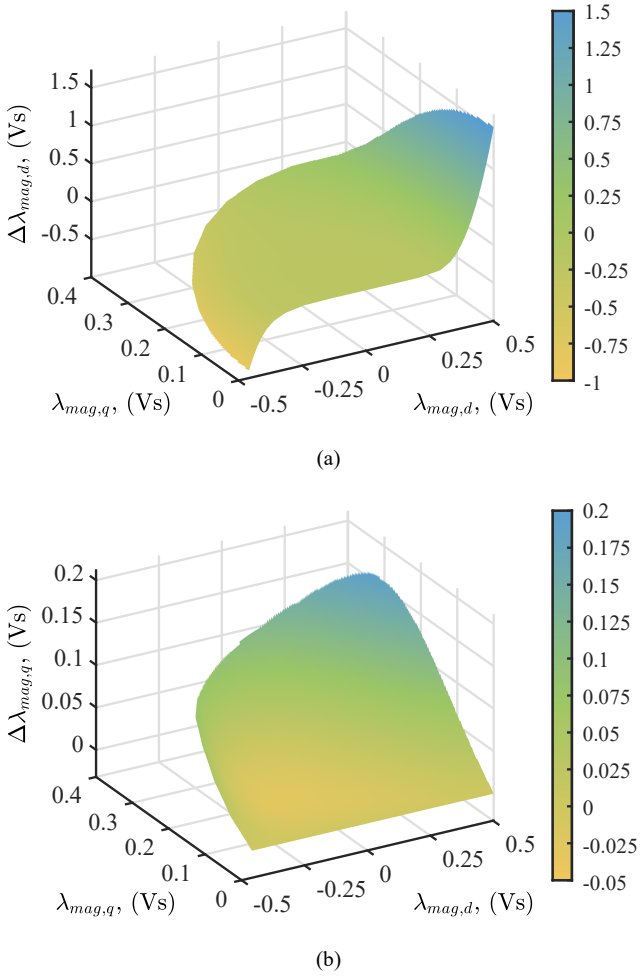

Fig. 5. Flux-errors for a positive rotor current: (a) for the d-axis, (b) for the q-axis.

approximates well the magnetizing flux linkage. Conversely, for higher $\lambda_{mag,d}$ values, which correspond to relatively high stator d-axis currents, the reference model derived in the unsaturated condition results in larger $\lambda_{mag,d}$. Therefore, according to (6), $\Delta\lambda_{mag,d}$ compensates for the deviation with the current-to-flux maps. Furthermore, the cross-saturation impact can be noted, as the flux-error values increase as $\lambda_{mag,q}$ rises, at a fixed $\lambda_{mag,d}$. Similar observations can be formulated for the q-axis flux-error map in Fig. 5b.

IV. Rotor Dynamic Model

In regard to the modeling of the rotor winding, neglecting the iron losses, the following equations are used:

$$v_f = \mathrm{R_f}\, i_f + \frac{d\lambda_f}{dt} \tag{12}$$

$$\lambda_f = \mathrm{L_{\sigma f}}\, i_f + \lambda_{f,mag} \tag{13}$$

where v_f, i_f and λ_f are the voltage, current and flux linkage of the field winding, respectively, while $\mathrm{R_f}$ is the resistance and $\mathrm{L_{\sigma f}}$ is the leakage inductance. $\lambda_{f,mag}$ is the rotor magnetizing

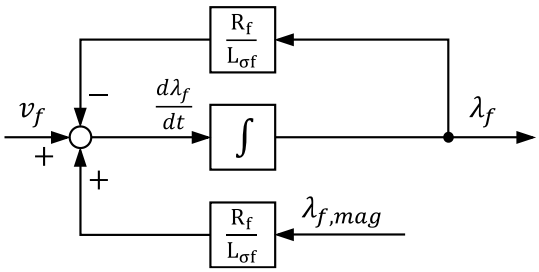

Fig. 6. Electromagnetic model of the field winding.

flux linkage, which is generated by the combined action of the stator and rotor windings.

In a similar way to the stator approach, the expression of the field current obtained by means of (13) can be replaced into (12), leading to (14). The model schematic representation is presented in Fig. 6.

$$\frac{d\lambda_f}{dt} = v_f + \frac{R_f}{L_{\sigma f}}\lambda_{f,mag} - \frac{R_f}{L_{\sigma f}}\lambda_f \tag{14}$$

In order to implement the field winding model including the iron saturation nonlinearities, the rotor current-to-flux map (15) is used, along with the corresponding magnetizing flux linkage map (16).

$$\lambda_f = \lambda_f\left(\sum_k i_{d,k}, \sum_k i_{q,k}, i_f\right) \tag{15}$$

$$\lambda_{f,mag} = \lambda_f\left(\sum_k i_{d,k}, \sum_k i_{q,k}, i_f\right) - L_{\sigma f}\, i_f \tag{16}$$

During the numerical simulations, the rotor magnetizing flux linkage, which is a function of all the stator *d*- and *q*- currents in the units and of the rotor current, can be expressed as:

$$\lambda_{f,mag} = \lambda_{fs} + M_f\, i_f - \Delta\lambda_{f,mag} \tag{17}$$

in which the terms in the right-hand side are determined with a similar procedure to the stator model. In this regard, the rotor flux linkage λ_{fs} generated by the stator windings is derived as:

$$\lambda_{fs} = \lambda_f\left(\sum_k i_{d,k}, \sum_k i_{q,k}, 0\right) \tag{18}$$

while the rotor magnetizing inductance M_f corresponds to:

$$M_f = \frac{\lambda_{f,mag}\left(\sum_k i_{d,k}, \sum_k i_{q,k}, i_f\right) - \lambda_{fs}}{i_f} \tag{19}$$

The considerations formulated for the determination of the stator magnetizing inductances in different operating conditions remain valid also for the rotor case (19). The computation of M_f in the unsaturated condition represents a convenient choice, as it strongly affects the $\Delta\lambda_{f,mag}$ values, improving the accuracy of the model at the borders of the maps. Moreover, similarly to the stator modeling approach, the sum of (18) with the magnetizing inductance contribution will hereinafter be referred to as *'rotor reference model'*, which intrinsically deviates from the map in (16) depending on the operating point of the machine.

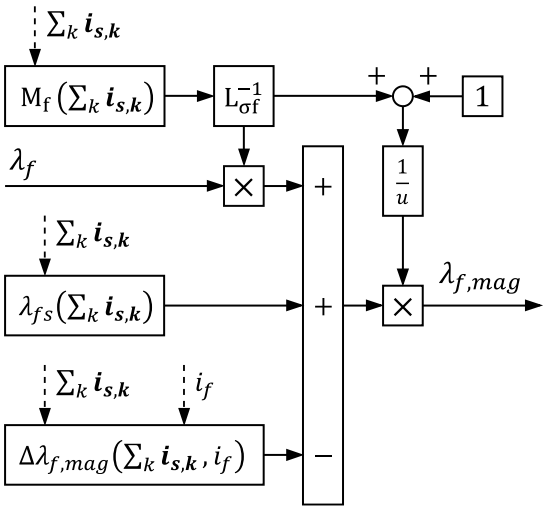

Fig. 7. Computation of the rotor magnetizing flux linkage.

Finally, $\Delta\lambda_{f,mag}$ is the flux-error map for the field winding, compensating for the deviation between rotor reference model and magnetizing flux linkage. Differently from the stator model, the rotor flux-error map can be directly expressed as a function of the machine currents in the simulation environment. Indeed, since the field winding modeling relies on scalar equations, the flux-error map approach is more straightforward than the one of the stator, with $\Delta\lambda_{f,mag}$ not requiring the normalization [29]. In this case, starting from (17), the flux-error map for the rotor can be determined as in (20) for a domain of equally spaced currents.

$$\Delta\lambda_{f,mag} = \Delta\lambda_{f,mag}\left(\sum_k i_{d,k}, \sum_k i_{q,k}, i_f\right) \tag{20}$$

In order to complete the model, the field current, determined by means of (13), can be substituted into (17), leading to:

$$\lambda_{f,mag} = \frac{1}{Y+1}\left(Y\lambda_f + \lambda_{fs} - \Delta\lambda_{f,mag}\right) \tag{21}$$

where $Y = (M_f\, L_{\sigma f}^{-1})$ for clarity reasons. The corresponding scheme is provided in Fig. 7, in which the stator current impact on the rotor approach can be noted. In addition, the field current from the previous time instant must be used for the solution, to interpolate the maps of the flux-error approach. Furthermore, the i_f from the previous simulation step constitutes also an input of the stator model, as it can be seen in Fig. 3.

A possible alternative to the rotor flux-error map approach is based on the inversion of (15), as thoroughly presented in [26]. In this case, the relationship in (22) is computed for a domain of regularly spaced current and flux values using the field winding current-to-flux map, for a computationally efficient model. The use of the field current from the previous time instant is needed also for this alternative approach, which is equivalent to the one with the flux-error map in terms of results accuracy.

$$i_f = i_f\left(\sum_k i_{d,k}, \sum_k i_{q,k}, \lambda_f\right) \tag{22}$$

In both cases, the separate rotor block in the dynamic model of the EESM, interacting by means of the currents with the stator one, provides enhanced simulation capabilities [26]. Indeed, the

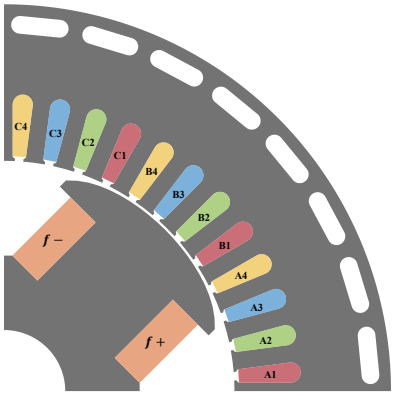

Fig. 8. Cross-section of the quadruple-three-phase EESM.

overvoltage induced in the field winding due to a sudden stator current variation can be simulated using the separate block, by acting directly on the stator current at the input of the block.

V. Simulation Results

The developed modular modeling approach for multi-three-phase EESMs has been analyzed in the simulation environment using the data coming from a quadruple-three-phase prototype, whose cross-section is represented in Fig. 8. The machine model parameters and the current-to-flux relationships needed for the flux-error maps have been obtained by means of finite element analyses. For the four stator three-phase sets, the same $R_{s,k}$ and $L_{\sigma s,k}$ values have been used. In addition, the current ratings of each stator three-phase set and of the field winding are 75 A and 13 A, respectively. Although the model numerical efficiency has been optimized by means of the interpolation of the flux-error maps, simulations have been performed for stator currents up to 73.5 A in each set, so as to exclude the errors at the borders of the multidimensional maps from the results.

In order to analyze the accuracy of the results and simulation capabilities of the developed multi-three-phase EESM modular model, the scheme in Fig. 9 has been implemented. The adopted procedure is based on the closed-loop flux control of the stator three-phase units and of the rotor winding. For the simulation, sinusoidal reference currents are generated for each stator set and for the rotor winding. In this analysis, it has been chosen to use the same current components for all the stator sets, without compromising the validity of the obtained results. Moreover, the current waveforms have different frequencies, so as to include many possible combinations in the simulation. The reference current $\boldsymbol{i}^*_{\boldsymbol{s,k}}$ for the stator k-th set and the reference current i^*_f for the rotor winding are shown in Fig. 10a. The generated currents are the input for the machine current-to-flux maps, to determine the reference flux linkages $\boldsymbol{\lambda}^*_{\boldsymbol{s,k}}$ and λ^*_f. The currents and fluxes allow also retrieving the corresponding reference torque $T^*_{e,k}$ for each stator three-phase set, whose value is depicted in Fig. 10b.

In this scenario, the closed-loop control of the flux linkages is achieved by means of PI regulators. The output voltages $\boldsymbol{v}_{\boldsymbol{s,k}}$ and v_f allow imposing the fluxes in the stator and rotor models. Moreover, the electrical pulsation ω_e for the stator sets varies as in Fig. 10c, to further analyze the numerical performance of the proposed modeling approach. The current interruption in one set

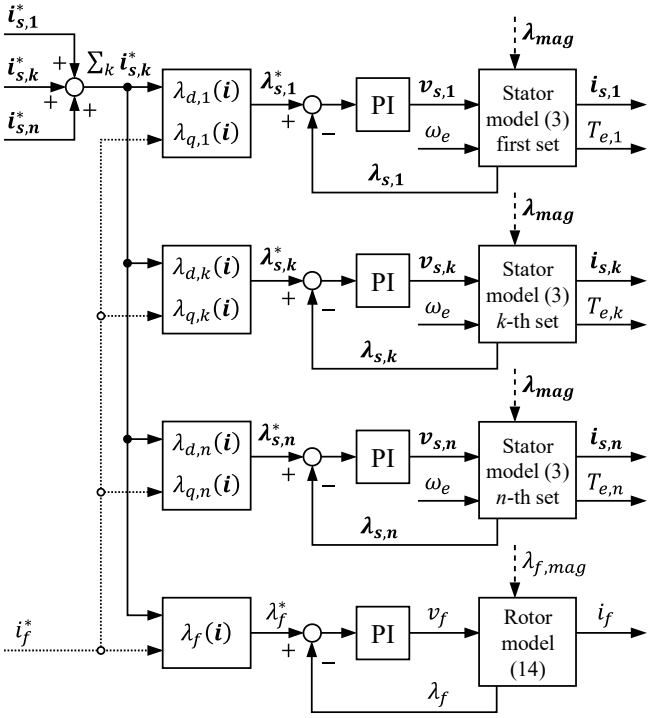

Fig. 9. Scheme of the closed-loop flux control.

at a time is also simulated, excluding a stator unit every 5 s with additional random delays, to evaluate the accuracy of the model in representing fault conditions. The number of stator active sets is also reported in Fig. 10c. Finally, the currents of the stator and rotor models and the torque produced by each set are compared to the reference ones to evaluate the results accuracy.

For the comparison of the stator variables with the reference ones, the three-phase set which remains active through the entire simulation is chosen as representative of the model performance, as the active stator sets have the same reference variables. The differences between the reference and model currents are shown in Fig. 10d, while the torque difference for the considered set is presented in Fig. 10e. The differences are indicated by $\varepsilon_{d,k}$ and $\varepsilon_{q,k}$ for the stator current components, by ε_f for the rotor current and by $\varepsilon_{T,k}$ for the torque. Considering the errors magnitudes, it could be concluded that excellent agreement is obtained for the model currents and torque, while the spikes in the differences correspond only to the first few instants following the openings of the stator sets. In this framework, the developed modeling approach based on the flux-error maps formulation presents high fidelity in representing the iron saturation effects related to large currents, as well as in simulating the electromagnetic dynamics when one or more three-phase sets are in open-circuit.

VI. Conclusion

A modular dynamic model for multi-three-phase electrically excited synchronous machines has been developed. The multi-stator approach interacts with a separate field winding model by means of the currents. The iron saturation and the corresponding nonlinear relationships between the machine currents and flux linkages are considered using flux-error maps, both for the stator three-phase sets and for the rotor winding.

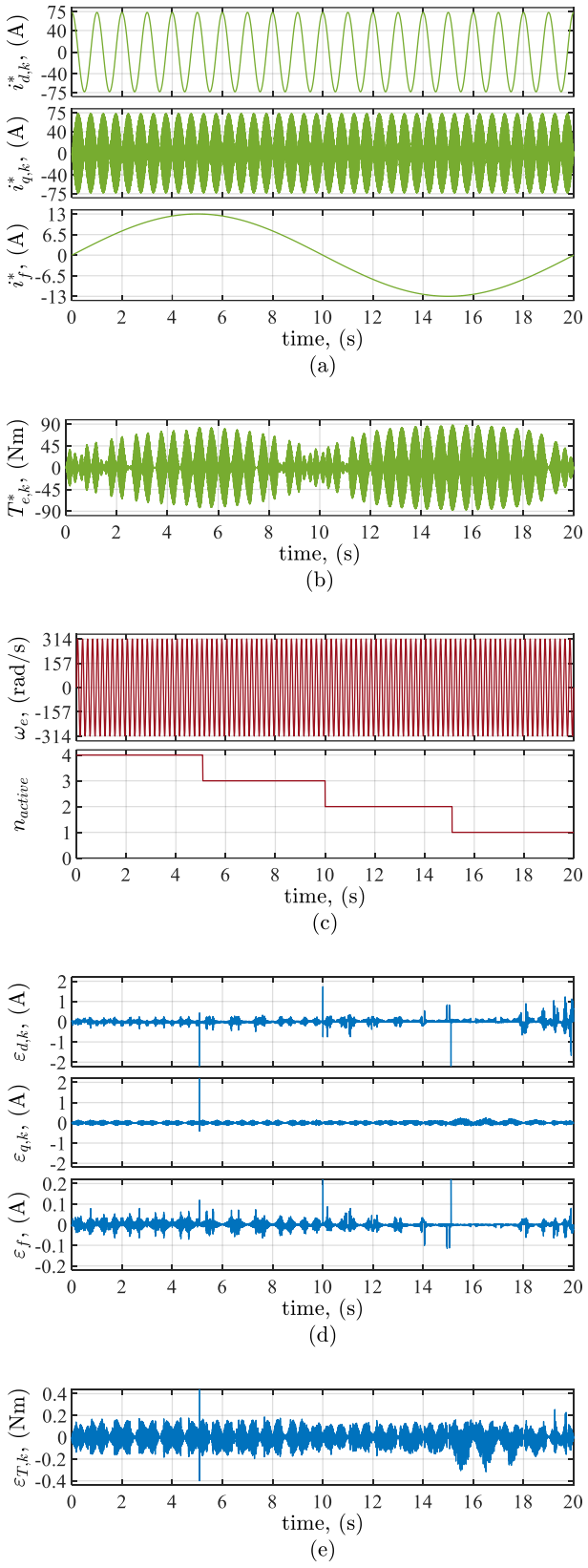

Fig. 10. Simulation results: (a) reference currents waveforms, (b) reference torque, (c) electrical pulsation and number of active sets, (d) current errors, (e) torque error.

The MS formulation allows distinguishing the contribution of each set to the magnetizing flux linkage and machine torque. Moreover, different resistance and leakage inductance values for the stator sets can be considered in the model. Furthermore, the convenient representation of fault conditions in the simulation is also achieved, thanks to the definition of the stator magnetizing flux linkage. Regarding the rotor modeling, the field flux linkage dynamics is computed in a separate block. The corresponding rotor current is also used in the interpolation of the stator model maps, to consider the effects of the variable excitation field.

The numerical validation of the proposed multi-three-phase EESM model has been performed in a simulation environment using the data of a quadruple-three-phase prototype, which have been derived by means of finite element analyses. The accuracy of the results for the closed-loop flux control has illustrated the high fidelity achievable with the proposed model in representing the machine electromagnetic dynamics, for both the healthy and faulty conditions. The subsequent development of the presented work will focus on the model experimental validation and on the application of the flux-error maps formulation to the nonlinear dynamic modeling of conventional three-phase machines.

ACKNOWLEDGMENTS

The activities conducted by Lorenzo Perilli for this publication are part of the project PNRR-NGEU which has received funding from the MUR-DM 117/2023.

This study was carried out within the MOST – Sustainable Mobility National Research Center and received funding from the European Union Next-GenerationEU (PIANO NAZIONALE DI RIPRESA E RESILIENZA (PNRR) – MISSIONE 4 COMPONENTE 2, INVESTIMENTO 1.4 – D.D. 1033 17/06/2022, CN00000023). This manuscript reflects only the authors' views and opinions, neither the European Union nor the European Commission can be considered responsible for them.

REFERENCES

[1] A. G. Yepes *et al.*, "Per-Phase Stator-Resistance Estimation by DC-Signal Injection in Open-Phase Fault-Tolerant Six-Phase Induction Motor Drives," in *IEEE Transactions on Industrial Electronics*, vol. 72, no. 2, pp. 1101-1112, Feb. 2025.

[2] F. Baneira, J. Doval-Gandoy, A. G. Yepes, Ó. López and D. Pérez-Estévez, "Control strategy for dual three-phase PMSMs with minimum losses in the full torque operation range under single open-phase fault," 2016 IEEE Energy Conversion Congress and Exposition (ECCE), Milwaukee, WI, USA, 2016, pp. 1-8.

[3] M. Alnajjar and D. Gerling, "Six-phase electrically excited synchronous generator for More Electric Aircraft," 2016 International Symposium on Power Electronics, Electrical Drives, Automation and Motion (SPEEDAM), Capri, Italy, 2016, pp. 7-13.

[4] M. Alnajjar and D. Gerling, "Model predictive control of six-phase variable frequency electrically excited starter generator for more electric aircraft," 2015 IEEE 11th International Conference on Power Electronics and Drive Systems, Sydney, NSW, Australia, 2015.

[5] J. Wang, R. Qu, Y. Liu and J. Li, "Study of Multiphase Superconducting Wind Generators With Fractional-Slot Concentrated Windings," in *IEEE Transactions on Applied Superconductivity*, vol. 24, no. 3, pp. 1-6, June 2014, Art no. 5202106.

[6] J. Wang, R. Qu and Y. Liu, "Comparison Study of Superconducting Generators With Multiphase Armature Windings for Large-Scale Direct-Drive Wind Turbines," in *IEEE Transactions on Applied Superconductivity*, vol. 23, no. 3, pp. 5201005-5201005, June 2013, Art no. 5201005.

[7] S. Rubino, I. R. Bojoi, F. Mandrile and E. Armando, "Modular Stator Flux and Torque Control of Multi-Three-Phase Induction Motor Drives," in *IEEE Transactions on Industry Applications*, vol. 56, no. 6, pp. 6507-6525, Nov.-Dec. 2020.

[8] E. Jung, H. Yoo, S. -K. Sul, H. -S. Choi and Y. -Y. Choi, "A Nine-Phase Permanent-Magnet Motor Drive System for an Ultrahigh-Speed Elevator," in *IEEE Transactions on Industry Applications*, vol. 48, no. 3, pp. 987-995, May-June 2012.

[9] A. Gneiting and N. Parspour, "Multi-Objective Optimization of a Quadruple 3-Phase Inductive Electrically Excited Synchronous Machine for 48V Traction Drives," IECON – 47th Annual Conference of the IEEE Industrial Electronics Society, Toronto, ON, Canada, 2021, pp. 1-6.

[10] S. Rubino, F. Mandrile, E. Armando, I. R. Bojoi and L. Zarri, "Fault-Tolerant Torque Controller Based on Adaptive Decoupled Multi-Stator Modeling for Multi-Three-Phase Induction Motor Drives," in *IEEE Transactions on Industry Applications*, vol. 58, no. 6, pp. 7318-7335, Nov.-Dec. 2022.

[11] E. Levi, "Multiphase Electric Machines for Variable-Speed Applications," in *IEEE Transactions on Industrial Electronics*, vol. 55, no. 5, pp. 1893-1909, May 2008.

[12] C. Bassi, A. Tessarolo, R. Menis and G. Sulligoi, "Analysis of different system design solutions for a high-power ship propulsion synchronous motor drive with multiple PWM converters," Electrical Systems for Aircraft, Railway and Ship Propulsion, Bologna, Italy, 2010, pp. 1-6.

[13] R. Kianinezhad, B. Nahid-Mobarakeh, L. Baghli, F. Betin and G. -A. Capolino, "Modeling and Control of Six-Phase Symmetrical Induction Machine Under Fault Condition Due to Open Phases," in *IEEE Transactions on Industrial Electronics*, vol. 55, no. 5, pp. 1966-1977, May 2008.

[14] A. Salem and M. Narimani, "A Review on Multiphase Drives for Automotive Traction Applications," in *IEEE Transactions on Transportation Electrification*, vol. 5, no. 4, pp. 1329-1348, Dec. 2019.

[15] W. Taha, P. Azer, A. D. Callegaro and A. Emadi, "Multiphase Traction Inverters: State-of-the-Art Review and Future Trends," in *IEEE Access*, vol. 10, pp. 4580-4599, 2022.

[16] M. J. Duran and F. Barrero, "Recent Advances in the Design, Modeling, and Control of Multiphase Machines—Part II," in *IEEE Transactions on Industrial Electronics*, vol. 63, no. 1, pp. 459-468, Jan. 2016.

[17] S. Rubino, R. Bojoi, D. Cittanti and L. Zarri, "Decoupled and Modular Torque Control of Multi-Three-Phase Induction Motor Drives," in *IEEE Transactions on Industry Applications*, vol. 56, no. 4, pp. 3831-3845, July-Aug. 2020.

[18] X. Jiang, W. Huang, R. Cao, Z. Hao and W. Jiang, "Electric Drive System of Dual-Winding Fault-Tolerant Permanent-Magnet Motor for Aerospace Applications," in *IEEE Transactions on Industrial Electronics*, vol. 62, no. 12, pp. 7322-7330, Dec. 2015.

[19] F. Barrero and M. J. Duran, "Recent Advances in the Design, Modeling, and Control of Multiphase Machines—Part I," in *IEEE Transactions on Industrial Electronics*, vol. 63, no. 1, pp. 449-458, Jan. 2016.

[20] F. Scuiller, J. -F. Charpentier and E. Semail, "Multi-star multi-phase winding for a high power naval propulsion machine with low ripple torques and high fault tolerant ability," 2010 IEEE Vehicle Power and Propulsion Conference, Lille, France, 2010.

[21] W. Bian, Z. Zhang, L. Li, C. Jin, J. Li and F. Guo, "An Approximate Three-Phase AC Excitation Method With Parallel Capacitors for Aircraft Wound Rotor Synchronous Starter/Generator," in *IEEE Transactions on Transportation Electrification*, vol. 11, no. 2, pp. 5497-5508, April 2025.

[22] J. Tang, Y. Liu and N. Sharma, "Modeling and Experimental Verification of High-Frequency Inductive Brushless Exciter for Electrically Excited Synchronous Machines," in *IEEE Transactions on Industry Applications*, vol. 55, no. 5, pp. 4613-4623, Sept.-Oct. 2019.

[23] F. Yao, Q. An, L. Sun and T. A. Lipo, "Performance Investigation of a Brushless Synchronous Machine With Additional Harmonic Field Windings," in *IEEE Transactions on Industrial Electronics*, vol. 63, no. 11, pp. 6756-6766, Nov. 2016.

[24] T. Xiao, Z. Ran, Z. Q. Zhu, D. Liang and P. Wang, "Optimal Stator/Rotor Copper Loss Ratio for Maximum Torque of Electrically Excited Machines," in *IEEE Transactions on Industry Applications*, vol. 61, no. 1, pp. 137-150, Jan.-Feb. 2025.

[25] F. Graffeo, S. Vaschetto, S. Rubino, A. Tenconi and A. Cavagnino, "Fast Computation of the No-Load Characteristic for Wound Field Synchronous Propulsion Motors," in *IEEE Transactions on Transportation Electrification*, vol. 11, no. 1, pp. 4111-4120, Feb. 2025.

[26] L. Perilli, F. Graffeo, S. Rubino and S. Vaschetto, "Dynamic Models for Electrically Excited Synchronous Machines based on Flux-to-Current and Current-to-Inductance Maps," 2024 IEEE Energy Conversion Congress and Exposition (ECCE), Phoenix, AZ, USA, 2024, pp. 5588-5595.

[27] J. -H. Lee, Y. -C. Kwon and S. -K. Sul, "High-Fidelity Induction Motor Simulation Model Based on Finite Element Analysis," in *IEEE Transactions on Industrial Electronics*, vol. 69, no. 10, pp. 9872-9883, Oct. 2022.

[28] M. Slunjski, O. Dordevic, M. Jones and E. Levi, "Symmetrical/Asymmetrical Winding Reconfiguration in Multiphase Machines," in *IEEE Access*, vol. 8, pp. 12835-12844, 2020.

[29] C.-M. Ong, "Dynamic Simulation of Electric Machinery: Using Matlab/Simulink," Prentice Hall, 1997.

[30] S. Rubino, L. Tolosano, F. Mandrile, E. Armando and R. Bojoi, "Flux Polar Control (FPC): A Unified Torque Controller for AC Motor Drives," in *IEEE Transactions on Industry Applications*, vol. 59, no. 4, pp. 4140-4163, July-Aug. 2023.